Sedimentologika

10.57035/journals/sdk.2026.e42.2385

Integrating field-based and digital datasets to improve geometric accuracy of geologic cross sections constructed from outcrop

Thomas G. E. Peploe* [1,2], **Paul R. Nesbit** [1,3], **Rebecca G. Englert** [1,4], **Miquel Poyatos-Moré** [5], **Brian W. Romans** [6], **Lisa Stright** [7], **and Stephen M. Hubbard** [1]

[1]Department of Earth, Energy, and Environment, University of Calgary, AB, Canada
[2]Canadian Natural Resources Ltd., Calgary, AB, Canada
[3]Department of Environmental Sciences, University of San Francisco, CA, U.S.A.
[4]MBARI, Monterey Bay Aquarium Research Institute, Moss Landing, CA, U.S.A.
[5]Departament de Geologia, Universitat Autònoma de Barcelona, Spain
[6]Department of Geosciences, Virginia Tech, Blacksburg, VA, U.S.A.
[7]Warner College of Natural Resources, Colorado State University, CO, U.S.A.

CRediT statement: *Writing-original draft*: TGEP, PRN, RGE. *Writing-review & editing*: TGEP, PRN, RGE, BWR, LS, SMH. *Visualization*: TGEP. *Conceptualization*: TGEP, PRN, RGE. *Formal analysis*: TGEP, PRN, RGE, BWR. *Investigation*: TGEP, MP-M, BWR, SMH. *Methodology*: LS, PRN, RGE.

*Corresponding authors: Thomas G. E. Peploe, thomas.peploe@ucalgary.ca

Abstract

Outcrop exposures of sedimentary rocks preserve vital records of depositional processes and offer key insights into Earth's depositional history. Traditional field-based techniques, such as measuring bed orientations, sketches, and field photography, have long been used to document stratigraphic patterns, while modern approaches now leverage high-resolution panoramas and drone-based photogrammetry to quantify and geolocate measurements. Although Digital Outcrop Models (DOMs) derived from UAVs (drones) markedly improve our ability to capture and interpret spatial details, these modern approaches, when used to generate 2-D stratigraphic correlation panels, are still challenged by distortions caused by outcrop perspective and structural deformation. To accurately constrain stratigraphic reconstructions derived from DOMs, calibrated field data is necessary to corroborate these observations with thicknesses, length scales, and lithologies. Here, we present a method to correct stratigraphic interpretations from DOMs for structural overprint and outcrop perspective using field-based paleocurrent and strike-and-dip measurements to produce geometrically accurate surface length, height, and dip in stratigraphic correlation panels. We demonstrate this method on Cerro Cazador, a 15 kilometer-long outcrop transect in Patagonia, Chile, recognized as containing continental shelf and shelf-margin sedimentary deposits. By systematically comparing three data projection strategies: no correction, a single correction, and a novel multi-correction workflow that applies localized adjustments to distinct structural regions, we show that the multi-correction method yields depositional geometries consistent with expected stratigraphic patterns (e.g., flat topset and bottomset deposits, sloping foresets, shelf-edge trajectories). These findings underscore the need for incorporating field-based calibrations into drone-derived models to accurately capture depositional patterns in geologically complex settings and highlight important implications for quantitative sedimentary analysis across diverse outcrop environments.

Research Article

Executive Editor
Stéphane Bodin

Associate Editor
Francisco Tognoli

Reviewers
two anonymous reviewers

Production Manager
Jarred Lloyd
Tom Dodd

Production Assistant
Matthew Wehner

Copy Editor
Elizabeth Mahon

Received: 2025-11-05
Accepted: 2026-04-08
Published: 2026-07-19

Keywords
digital outcrop models (DOMs)
drone photogrammetry
outcrop geology
stratigraphic interpretation
shelf-margin stratigraphy

This open access article © 2026 Peploe et al. is licensed under the CC BY 4.0 license.

Plain language summary

Drone-based data collection has transformed how geologists study rock outcrops by creating detailed digital reconstructions of large and often inaccessible exposures called Digital Outcrop Models (DOMs). They capture fine-scale details and enable accurate measurements of ancient sedimentary rock exposures. However, outcrops are commonly deformed, and distortions caused by perspective, folding or geological tilting can make the resulting models difficult to interpret if not corrected. This study presents a new approach that combines field measurements with drone-based models to correct for these distortions and produce more accurate representations of depositional stratigraphy. Using an extensive 15 kilometer-long outcrop in southern Chile, we show that simplistic, yet commonly used, methods can oversimplify complex structures, while our new multi-correction workflow better restores the original geometry of the strata. The corrected models reveal realistic sedimentary patterns, like flat shallow-marine deposits and inclined slope deposits, providing a clearer view of how sediments accumulated along ancient continental margins. By improving the accuracy of drone-derived reconstructions, this workflow enhances our ability to interpret how sedimentary systems evolved through time and offers a practical tool for geologists working in structurally complex or remote field areas.

1 Introduction

Outcrops of ancient sedimentary deposits are used to resolve past processes and environmental conditions, which contribute to paleoenvironmental and tectonic reconstructions (Mutti & Ricci-Lucchi, 1978; Posamentier & Walker, 2006; Rich, 1951). Interpretations of strata are commonly limited by outcrop scale, exposure, and continuity, and the inherent structural complexity that results from uplift and exhumation processes. Traditional field-based workflows that are used to characterize sedimentary outcrops often begin with the collection of measured sections, paleoflow data, and bedding orientations, followed by the generation of photopanels, which can be helpful when walking surfaces to correlate between sedimentary sections drawn on them. These methods can be limited by weather, inaccessible outcrops on areas like cliff-faces, low-resolution photographs that may be taken with perspectives that fail to show depositional architectures, and an inability to capture the changing perspective of a 3-D rock-face. Ultimately, these factors may inhibit accurate data collection, leading to issues when quantifying architectural relationships, and scales over extensive, km-long outcrops. To accurately constrain DOM-derived stratigraphic reconstructions in the presence of outcrop perspective distortions and structural overprints, ground-based calibrated field-data is necessary (Figure 1B). Here, structural overprint includes spatial variations in bedding attitude (strike and dip), and deformation-driven modification of bed geometry (e.g., folding, faulting, and penetrative strain such as layer-parallel shortening/extension) that can alter bed shape, continuity, apparent thickness, and length. Importantly, these effects are not unique to DOM-based analysis, but reflect the fundamental limitation that both digital and traditional field observations are restricted to the exposed surface expression of the outcrop.

In the past several decades, high-resolution aerial photography (e.g., Google Earth Pro) and LiDAR (light detection and ranging) have been incorporated into traditional field-based workflows to constrain and generate 3-D digital models of outcrops (Bellian et al., 2005; Enge et al., 2007; Hodgetts, 2013; Pringle et al., 2006). More recently, the advent of digital outcrop models (DOMs) derived from uncrewed aerial vehicles (UAVs or drones) provide a more accurate perspective of large, often inaccessible, outcrops. These DOMs have been implemented in virtual geologic field trips (McCaffrey et al., 2010), geohazard assessments, (Kucharczyk & Hugenholtz, 2021; Niethammer et al., 2012), archaeology (Campana, 2017; Magnani et al., 2020), mineral exploration and mine planning (Honarmand & Shahriari, 2021; Park & Choi, 2020; Shahmoradi et al., 2020), volcanic hazard monitoring (Wakeford et al., 2019), environmental change monitoring (Honarmand & Shahriari, 2021; Kirsch et al., 2018; Sikakwe, 2023), and stratigraphic reconstructions (Englert et al., 2018; Nesbit et al., 2018; Nieminski & Graham, 2017). DOMs are also widely used in structural geology to quantify fault and fold geometries and fracture network attributes, enabling kinematic and strain interpretations from inaccessible exposures (e.g., Bemis et al., 2014; Bistacchi et al., 2015; Casini et al., 2016; Jones et al., 2009). Drone-based field surveys often photograph surface details over

extensive areas (Chesley et al., 2017; Durkin et al., 2020), offering enhanced visibility to areas that vary in size (cm to km), types of geological features (e.g., folds, faults, and slumps), outcrop perspectives (e.g., 2-D, 3-D, incomplete, or oblique exposures), or accessibility (e.g., cliff faces). Recent studies have demonstrated how a DOM can be used to resolve outcrop stratigraphy, by correlating bedding planes and sedimentary packages across widely spaced outcrops (Coutts et al., 2024; Nesbit et al., 2021). However, while DOMs capture the outcrop characteristics, the interpretations of stratigraphic surfaces from them can be distorted by the structural overprint (strike and dip). A study by Cawood et al. (2017) found that while UAV surveys offer greater spatial coverage and enhanced structural characterization, they can also introduce notable uncertainties in orientation measurements if used in isolation. In this study, we aim to integrate the initial survey plans and data processing, with ground-based calibrations to correct for outcrop perspective distortions such that we can achieve more reliable structural and stratigraphic interpretations. Without correcting for the structural orientation, lineaments and surfaces on the DOM may contribute to the distortion of stratigraphic geometry and architecture (Figure 1C & D).

This study showcases a 22 km long outcrop of Upper Cretaceous strata in the Magallanes Basin at Cerro Cazador, southern Chile, spanning exposures that range from direct N-S orientations (dip-parallel) to oblique sections relative to the N-S trend. Previous regional stratigraphic studies in the basin have identified high-relief (kilometer-scale) sigmoidal clinoforms (Bauer et al., 2020; Daniels et al., 2019; Hubbard et al., 2010) in the stratigraphic transition between the Tres Pasos and Dorotea formations that are captured in a 15 km-long DOM at Cerro Cazador. The geometric characterization of these clinoforms, e.g., their length, height, and the dip angles of topsets, foresets, and bottomsets can be derived from observations made on the DOM. These form the basis for reconstructing stratigraphic profiles (Rich, 1951; Steel & Olsen, 2002), and the measurements of clinoform features underpin interpretations of shelf-to-basin relief, slope gradients, and water depth (Patruno et al., 2015; Patruno & Helland-Hansen, 2018; Pellegrini et al., 2020). To account for local structural variability in the outcrop and restore accurate depositional architecture, we develop an approach to calibrate the acquired drone-based DOM with ground-based field measurements. The objective is to validate and compare clinoform-surface geometry reconstructed from outcrop to measurements from modern and shallow subsurface datasets, and ultimately, to demonstrate a method to project and restore stratigraphic relationships for more reliable quantitative interpretations from outcrops.

2 Study Area

The Magallanes-Austral Basin is a NNW-SSE trending retroarc foreland basin that covers approximately 195 000 km^2 in southernmost South America (Sachse et al., 2016; Zambrano & Urien, 1970). This study focuses on exhumed shelf-margin deposits of the Tres Pasos Formation–Dorotea Formation transition at Cerro Cazador (Figure 2A; Bauer et al., 2020; Hubbard et al., 2010; Romans et al., 2010). Shelf-margins are defined as geomorphic breaks marking the transition from the gently dipping continental shelf to the steeper continental slope, often associated with significant changes in sedimentation style, gradient, and accommodation (Steel et al., 2000; Steel & Olsen, 2002). Strata at Cerro Cazador were deposited as prograding clinothem sediment packages, bound by sigmoidal clinoform surfaces, observed to have average paleoflow of 165° (n = 624) (Figure 2B). Clinoforms characteristically display sigmoidal geometries and are characterized by topsets (typically ~flat, uppermost surfaces), foresets (basinward-dipping slopes), and bottomsets (typically flat to shallowly dipping, lowermost surfaces), each representing distinct depositional environments within the sedimentary system (sensu Gilbert, 1885; Rich, 1951).

Clinoforms in the Dorotea and Tres Pasos formations (Figure 2C) have been mapped tens of kilometers into the basin through extensive field work validated by geochronological analyses (Figure 2D; Daniels et al., 2018, 2019). The Tres Pasos Fm. represents the upper-slope deposits of the Late Cretaceous system, and was deposited between 80.5 ± 0.3 and 77.4 ± 1.1 Ma (Figure 2C; Daniels et al., 2019). The overlying Dorotea Formation represents the coeval shelf deposits, and was deposited between 77.4 ± 1.1 and 67.1 ± 1.8 Ma (Figure 2C; Daniels et al., 2019). Bauer et al. (2020) established clinoform evolution utilizing outcrop photographs, field sketches, and high-resolution satellite imagery. Building on this foundation, Hage et al. (2022) quantified organic carbon burial within clinoform structures at Cerro

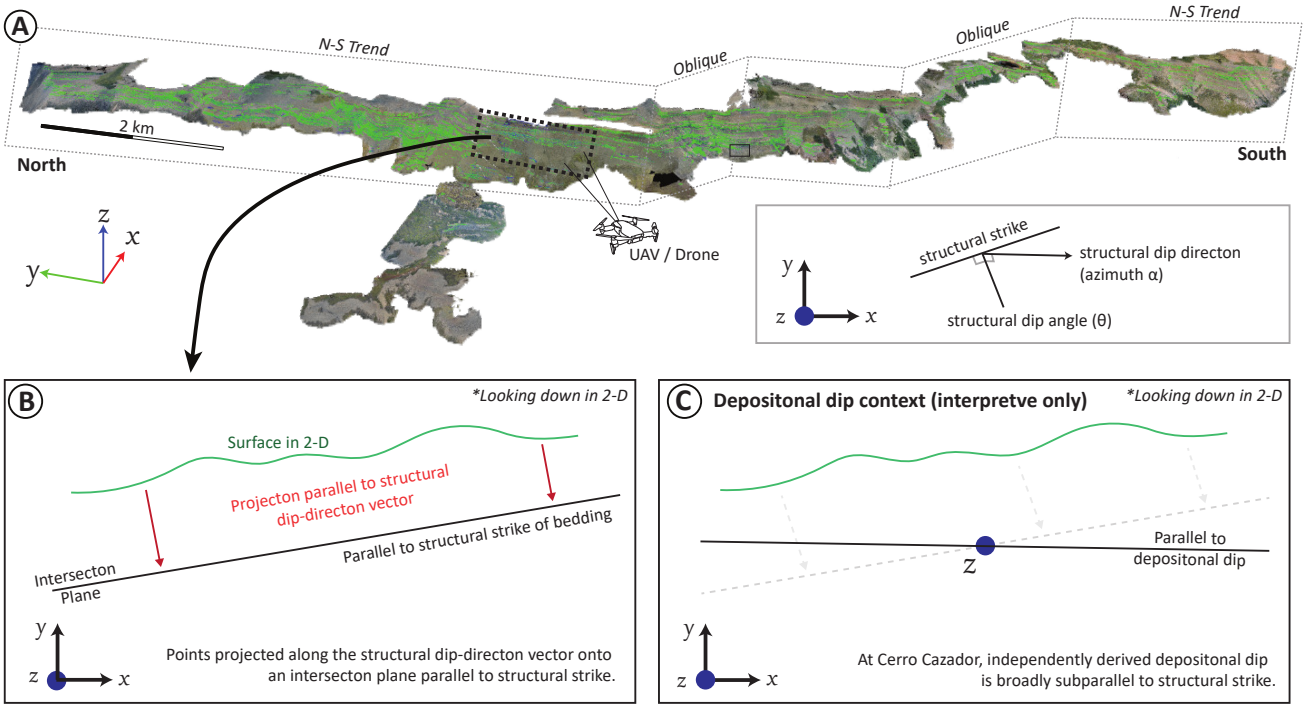

Figure 1 – The process for projecting interpreted surfaces on the digital outcrop model (DOM) captured by an unmanned aerial vehicle. **(A)** The full extent of the DOM (c. 15 km × 0.5 km) where green lines show the interpreted stratigraphic surfaces, made up of a series of points, digitized as polylines. **(B)** Schematic of the projection method used in this study, in which points are projected along the structural dip-direction vector onto an intersection plane parallel to structural strike. **(C)** Conceptual panel showing that independently derived depositional dip at Cerro Cazador is broadly subparallel to structural strike; this relationship provides depositional context only and is not an additional projection step.

Cazador, and was the first to use a DOM to constrain the outcrop.

Cerro Cazador contains several challenges for field-based mapping that can be minimized with drone-based methods, including (i) steep cliff locations, (ii) inaccessible private land, (iii) complex, large-scale sedimentologic features that are difficult to trace on the outcrop such as mass-wasting deposits that are characteristically convoluted and discordant with surrounding units (Bauer et al., 2020; Hage et al., 2022), and (iv) variations in localized strike and dip of bedding planes across the mountainside due to a combination of Cenozoic Andean tectonism, basin exhumation (Figure 2B; Wilson, 1991), eastward propagation of mountain building processes (Katz, 1963; Wilson, 1991), and/or syn-depositional or post-Miocene deformation (e.g., broad folds) associated with continued E-W Andean tectonism (Fosdick et al., 2011).

3 Data and Methodology

3.1 Digital Outcrop Model Generation

Following methods outlined in Nesbit et al. (2021) and Hage et al. (2022), a DJI Phantom 3 Professional quadcopter UAV was used to acquire images of the outcrop at central Cerro Cazador (c. 15 km-long ×0.5 km-thick succession) (Figure 2A & B). More than 19 500 images were obtained with primary camera angle perpendicular to outcrop exposure and additional images captured from above and at angles approximately 45° to the slope to increase coverage of complex outcrop faces and improve network geometry during photogrammetric processing (Nesbit et al., 2021; Nesbit & Hugenholtz, 2019). Initial drone flights were conducted in a grid pattern c. 20 to 30 m from the Cerro Cazador mountainside. These images were processed using SfM photogrammetry (Nesbit et al., 2021; Nieminski & Graham, 2017), and were divided into subsets (1 000 to 3 000 photos) to generate a DOM using Pix4D photogrammetric software. The DOM has a typical resolution of 0.03 to 0.04 m per pixel (Hage et al., 2022). Natural points on the outcrop were documented in the field using a differential-GPS (dGPS). These served as ground control points (GCP's; n = 30) in the photogrammetric process, providing constraints for scale, orientation, and positioning of the DOM.

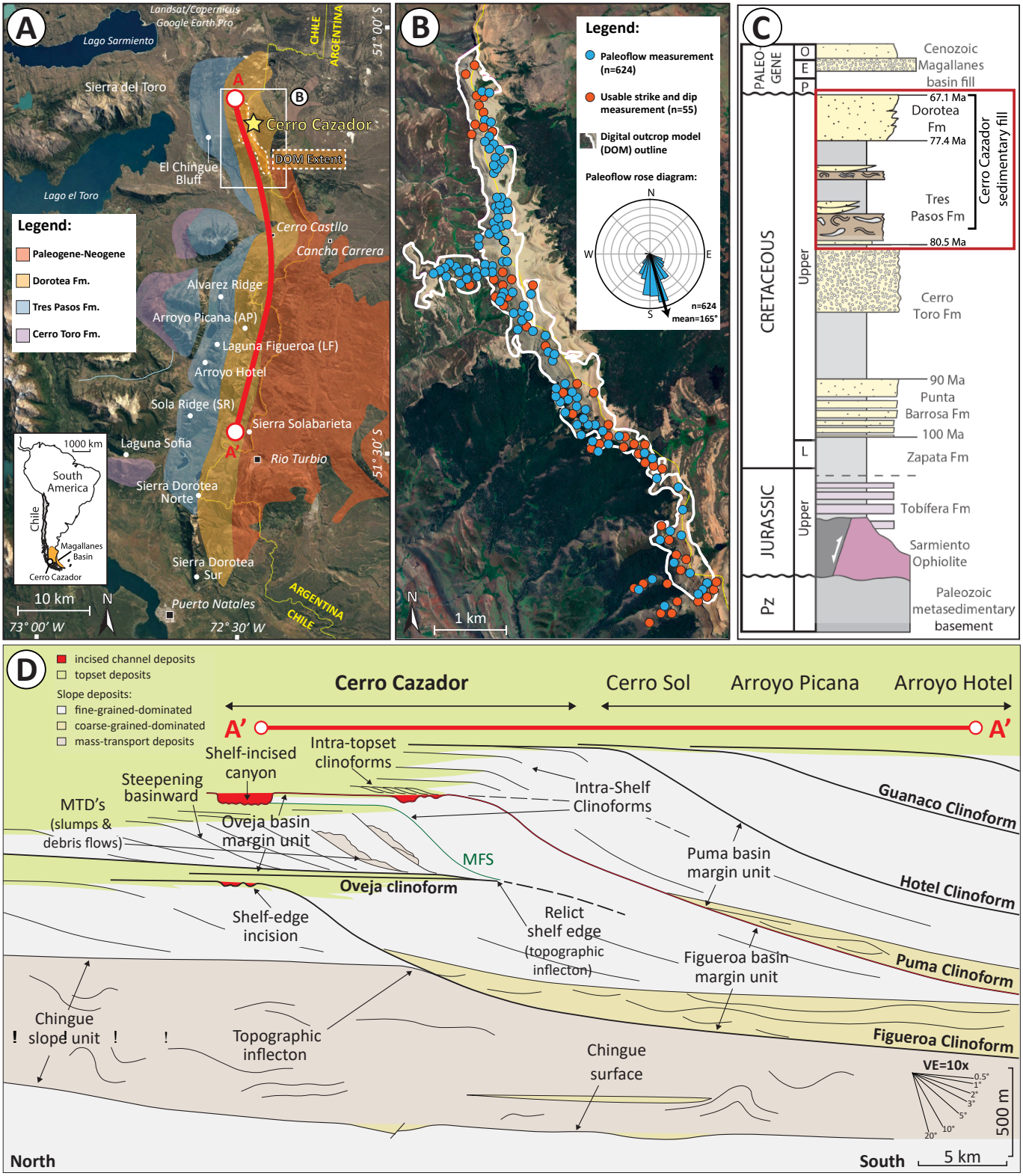

Figure 2 – **(A)** Satellite image of the eastern margin of the exhumed Magallanes Basin, southern Chile. The regional extent of the DOM at Cerro Cazador is shown in the north (Google Earth Pro). **(B)** Inset map of the Cerro Cazador study area showing the spatial distribution of paleoflow measurements (*n* = 624; blue), usable strike and dip measurements (*n* = 55; orange), and the outline of the digital outcrop model (DOM; white). **(C)** Stratigraphic column for the study area, with the coeval Late Cretaceous Tres Pasos and Dorotea formations highlighted in the red box (modified from Wilson, 1991; Fildani & Hessler, 2005; Fosdick et al., 2011; Schwartz et al., 2017; Daniels et al., 2019). Yellow represents sandstone, grey represents siltstone, brown represents mass-transport deposits, and pink represents igneous material. **(D)** Regional north-south cross-section of the basin oriented along depositional dip, from Cerro Cazador to Arroyo Hotel (adapted from Daniels et al., 2018; and Bauer et al., 2020)

3.2 Field Measurements

Strike and dip measurements (total n = 70) were collected in the field across the extent of the outcrop (Figure 2B). Some measurements were excluded as outliers if they were greater or less than 3 standard deviations from the mean (n = 15) (e.g. Renard et al., 2006; Thompson & Worden, 2017), or if they did not feature on the DOM (n = 21), leaving 55 useable strike and dip measurements (Figure 3A). These strike and dip data were then grouped based on their geographic and paleo-depositional context. Paleocurrent data recorded for this study (n = 624), and by Bauer et al. (2020) across Cerro Cazador, show a dominant south-southeastward orientation (165°; Figure 2B); which is interpreted to be representative of depositional dip. This paleoflow orientation is near parallel to the structural strike of the exhumed stratigraphy at Cerro Cazador, with subtle variation across the outcrop (Figure 2B). Four different groupings based on structural regions (North, Central, Bend, South) were defined by either large variations in neighboring strike and dip measurements or large distances (> 2 km) between data points (Figure 3A). For the North (n = 10), Central (n = 16), Bend (n = 12), and South (n = 17) structural regions, the average and standard deviations of their respective strikes/dips were calculated (Figure 3A & B). The resulting average strike and dip values were used for geometric correction of the photogrammetry model in those regions.

3.3 Defining Correction Regions

Deformation is spatially variable along long outcrop transects, like the one at Cerro Cazador, thus we implemented corrections using discrete structural regions representing kinematic blocks. Regions were initially qualitatively defined using the spatial locations of strikes and dips of bedding planes (Figure 3A), and then subsequently quantitatively refined by grouping those with similar strikes and dips (Figure 3B). We evaluated these regions iteratively, starting with a base case of a single correction (Figure 3C), and increasing domain count only when (i) corrected stratigraphic surfaces exhibited fewer non-geologic warps (e.g., unrealistic 'hinges', and overlapping surfaces), and (ii) the resulting depositional geometries were consistent with independent field constraints (e.g., expected consistent thickness trends and cross-section correlations). This subdivision was halted when additional domains produced only marginal improvement, which for this example at Cerro Cazador, was with four regions between 1.5 and 5.5 km long (Figure 3B & C).

Boundaries between regions (Figure 3A) were placed at laterally persistent step-changes in mean bedding attitude (distinct strike and dip clusters; between 1.5 to 5.5 km) identified from the spatial distribution of measurements (Figure 3A) and stereonet populations (Figure 3B). Regions were sufficiently constrained by measurement density and along-strike coverage (i.e., enough points to define a stable mean attitude; n > 10).

3.4 Data Interpretations and Projections

Features were digitized as polylines on the 3-D point cloud within Pix4D photogrammetry software following the methods of Nesbit et al. (2018) (Figure 3A). These included structural features (e.g., faults and folds), stratigraphic features (e.g., bedding planes, stratigraphic boundaries, unconformities), and sedimentary log locations. Measured sections were tied to the DOM using a dGPS, exported as shapefiles, including location attributes (x, y, z), and loaded into ArcGIS software. From there, data were projected onto a two-dimensional intersection plane.

The intersection plane is constructed from the measured structural dip direction (α) and structural dip angle (θ) (Figure 1B), which together define the normal vector to the plane. The plane follows the general equation:

$$Ax + By + Cz = D \tag{1}$$

where $A = sin(\alpha)$, $B = cos(\alpha)$, $C = -tan(\theta)$. The scalar D ensures that the plane passes through a specified origin point (x_0, y_0, z_0) satisfying the condition:

$$Ax_0 + By_0 + Cz_0 = D \tag{2}$$

This construction ensures that the plane is perpendicular to the dip vector and anchored in 3-D space. Importantly, features were projected orthogonally along the measured structural dip-direction vector (α, θ), which in this formulation define the normal vector of the plane. This projection returns the shortest-distance intersection of each point with the plane and provides a structurally corrected reference frame for reconstructing 2-D stratigraphic geometries. The workflow developed here primarily targets the orientation component of structural overprint (spatially variable rigid-body rotation/tilt of bedding

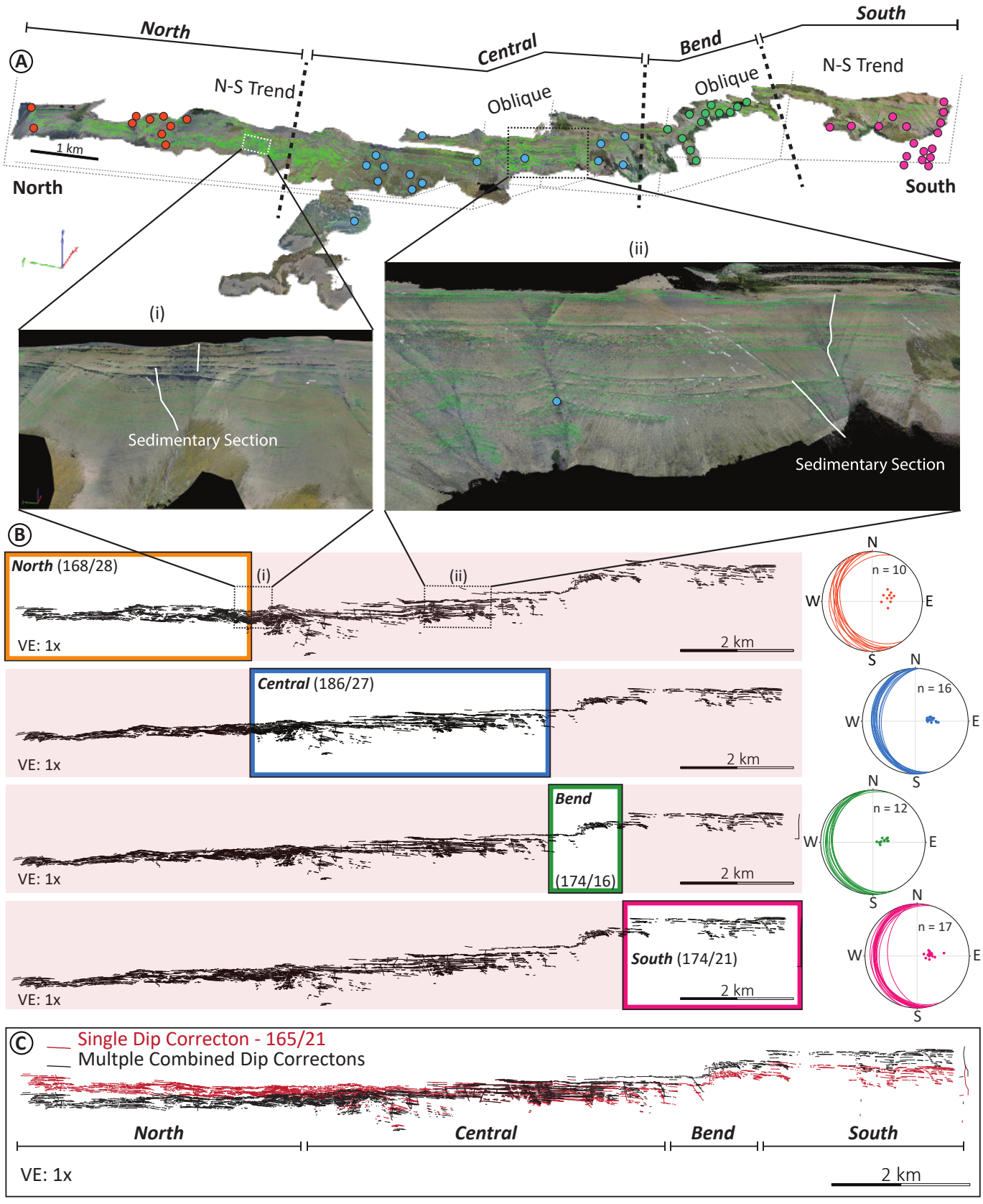

Figure 3 – **(A)** The full extent of the DOM (c. 15 km × 0.5 km) at Cerro Cazador with highlighted locations at the boundary between the North and Central structural regions (i), and at the central region over the boundary between oblique and N-S trending sections of the outcrop (ii). Locations of strike and dips across the outcrop are recorded, colored by their different structural region. **(B)** The four extracted, dip-corrections each applied to the entire cross-section, with areas outlined in rectangles showing where the projection was used to optimize stratigraphic geometries. Stereonets, showing planes of strikes and dips, of each region are shown alongside their averages and number of recordings. **(C)** Red lines on this figure represent single-dip corrections, to compare against the multiple-projection model of this study (black lines). The composite dip-corrected projection incorporates all of the corrected (orange, blue, green, and red) boxes from **(B)**. By manually combining the regions, more representative shelf-margin clinoform geometries and architectures are observed.

and regions) that biases apparent clinoform geometry in long outcrop transects. Although the intersection plane is defined from structural dip measurements, independently derived paleoflow measurements at Cerro Cazador indicate that depositional dip is broadly subparallel to structural strike (Figure 2B). This relationship provides depositional context for interpreting the corrected cross-sections, indicating they provide a depositional dip perspective (Figure 1C).

To reconstruct the original stratigraphic geometry of Cerro Cazador, we employed three different projection methods on the DOM and evaluated their effectiveness in representing stratigraphic structures. The first method applied no dip-projection corrections, where data were projected with a bedding strike orientation of 165° and no dip correction was used to preserve the raw observational data from the DOM, i.e., a vertical plane (Figure 1B). The second method utilized a single, uniform projection based on the regionally averaged strike and dip of 165°/21° documented by Bauer et al. (2020). The third method involved multiple localized projections as described in the second method, tailored to the four strike and dip regions identified within the outcrop (Figure 3B).

4 Results

4.1 No correction – strike of 165° and dip of 0°

4.1.1 Observations

Projected architectures of the extracted surfaces, lineaments, and sedimentary sections appeared to closely follow the topography at Cerro Cazador, e.g., uphill and convoluted geometries (Figure 4A). The surfaces in and around gullies often converged, overlapped, and had cross-cutting relationships (Figure 4A). The uncorrected projection yields a high frequency of overlapping surface points (n = 448; Figure 4A), reflecting widespread non-geologic surface convergence and crossover. The topset and foreset geometries of the clinoforms were often indistinguishable, making the shelf-margin architecture and trajectory impossible to analyze. Surfaces at the younger southern end of the outcrop projected stratigraphically beneath the older northern strata.

4.1.2 Interpretations

By only accounting for strike, the observed surfaces were effectively displayed as they would appear on satellite imagery (e.g., Google Earth) and field photographs. These surfaces were uncharacteristic of typical sigmoidal clinoforms, differing significantly from those observed in other ancient and modern systems (Patruno & Helland-Hansen, 2018). Clinoform trajectories at the southern end of the outcrop appeared to develop in a downstepping, or degradational pattern, which is inconsistent with previous descriptions of an aggradational to progradational shelf-margin evolution (Bauer et al., 2020; Daniels et al., 2019).

4.2 Single correction – strike of 165° and dip of 21°

4.2.1 Observations

A singular strike and dip projection of 165°/21° (Bauer et al., 2020) was applied to the observed surfaces (Figure 4B). This technique led to fewer overlapping and converging surfaces in gully regions relative to the uncorrected case (n = 7; Figure 4B), indicating fewer non-geologic surface crossovers under a single regional correction, but still represents inaccurately converging beds and remained difficult to distinguish between the topset and foreset geometries of the clinoforms as both had similar dip angles with no apparent shelf-slope break rollover zone. Where clinoform surfaces were identifiable, topset (c. 2.5 to 5.7°; Figure 4B) and foreset (6.9 to 10.7°) dip angles remained consistently steep, with dip-parallel topset bed thicknesses varying, implying incomplete restoration of originally sub-horizontal topset geometries. Mass-wasting deposits were characterized by discontinuous and convoluted bedding and were distinguishable from more organized strata (Moscardelli & Wood, 2008; Nieminski & Graham, 2017).

4.2.2 Interpretations

This method produces surfaces that are more congruent with established models of some shelf-margin features including flatter topsets, dipping foresets, discordant mass-wasting deposits, and the aggradational-to-progradational transition at the southern end of the transect (Bauer et al., 2020; Daniels et al., 2019), compared to the no correction method. Patruno & Helland-Hansen (2018) show how worldwide modern and ancient clinoforms often display a sigmoidal shape, however the ones geometrically corrected using this single projection at Cerro Cazador do not compare well to these examples. While this projection improved the clarity of overall stratal geometry, it also exaggerated the dip of all surfaces, including the relatively flat topsets, thereby

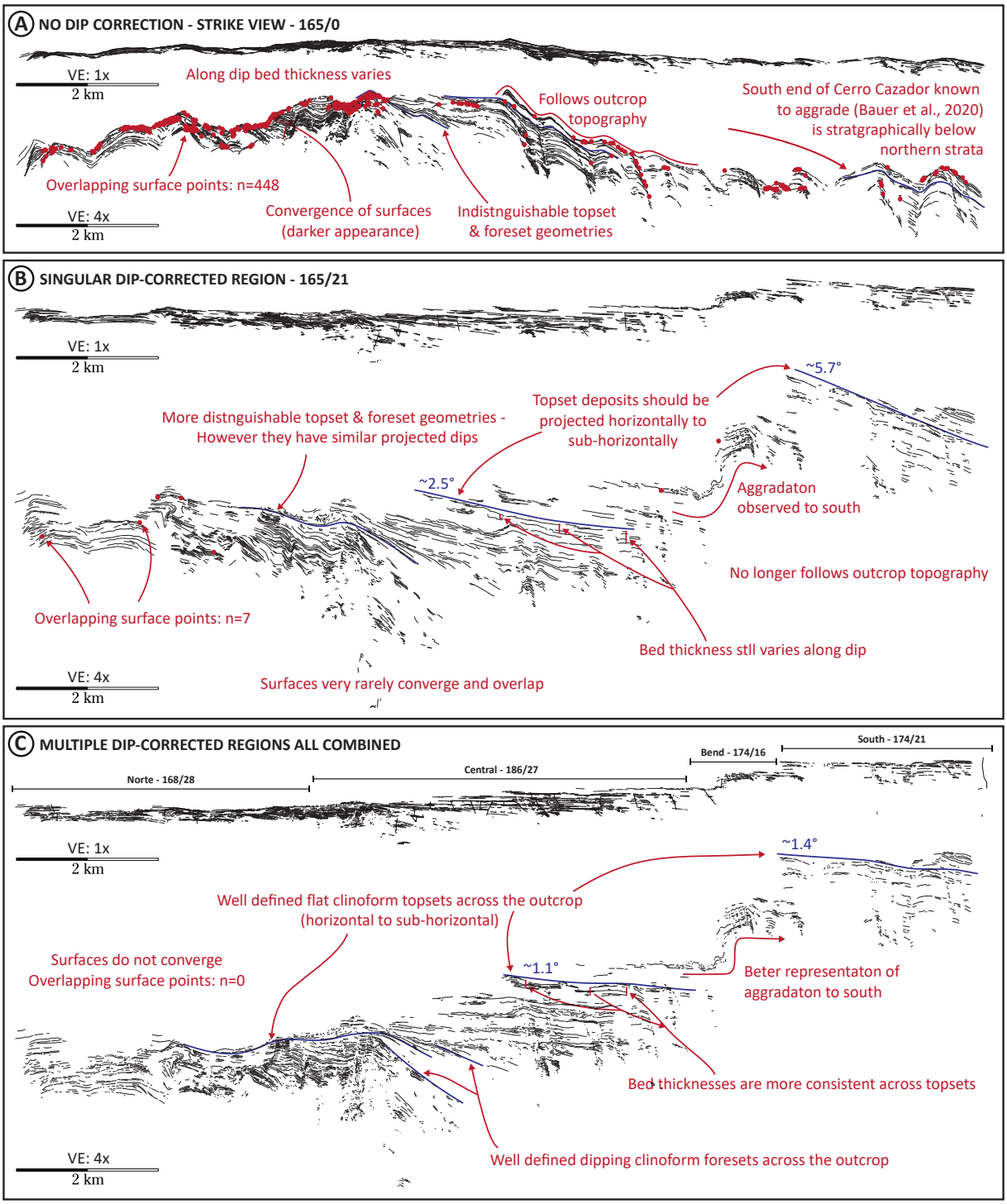

Figure 4 – Comparison of stratigraphic surfaces as revealed in the three projection methods described. **(A)** Uncorrected surfaces projected in a strike-parallel view, with a strike of 165° and a dip of 0°, showing geometries that follow outcrop topography rather than true depositional dip. This results in the convergence of surfaces, indistinguishable topset and foreset geometries, and misleading stratigraphic relationships (e.g., southern exposures appearing stratigraphically above northern strata). Overlapping surface points (n = 448) provide a semi-quantitative proxy for non-geologic surface convergence and crossover frequency in this projection. **(B)** Projection using a single structural correction – strike of 165° and dip of 21°, based on regional dip data (Bauer et al., 2020). This approach better reveals overall clinoform architecture and aggradational patterns to the south, but imposes an unrealistic southward dip on all surfaces, including clinoform topsets that should be horizontal to sub-horizontal. Overlapping surface points are reduced (n = 7), indicating partial convergence toward a stable solution, but annotated topset dip angles (c. 2.5 to 5.7°) and along-dip topset bed-thickness variability indicate incomplete restoration of original topset geometries. **(C)** Optimized multiple corrections – four region-specific strike and dip projections. This method produces a more geologically accurate cross section, with flat to gently dipping clinoform topsets, dipping foresets, and clearer representation of the transition to aggradational stacking in the southern part of the outcrop. In this multi-domain reconstruction, overlapping surface points are eliminated (n = 0), annotated topset dip angles are consistently sub-horizontal (c. 1.1 to 1.4°), and along-dip topset bed thicknesses are more laterally consistent, together indicating convergence and measurable improvement relative to simpler correction schemes.

complicating the recognition of trajectory transitions (Figure 4C). We therefore assume that these single geometric corrections were not entirely representative of their original depositional clinoformal geometries. Although possible, both clinoforms and mass-wasting deposits show very steep gradient ranges (6.9 to 10.7°), which are at the upper limit for recorded ancient shelf-margin clinoforms (Patruno et al., 2015). This has implications for over- and under-representing bed/package thicknesses, and sedimentary lithofacies distributions.

4.3 Multiple corrections – Four region-specific strike and dip projections

4.3.1 Observations

We applied four strike and dip projections of 168°/28°, 186°/27°, 174°/16°, and 174°/21° to the distinct outcrop regions from north-to-south across the outcrop (Figure 3B). This technique removed convoluted and discordant surfaces, and overlapping surface points are eliminated in the multi-domain reconstruction (n = 0; Figure 4C), providing a semi-quantitative indicator of reduced non-geologic surface crossover frequency. In this iteration, clear clinoform geometries are evident, with topset and foreset gradients of 1.1 to 1.4° and 6.7 to 10.2°, respectively, and topset bed thicknesses are more laterally consistent (Figure 4C). The aggradation-to-progradation clinoform trajectory trend at the southern end of the outcrop that was defined by Bauer et al. (2020) is apparent and comparable to other documented shelf-margin trends (e.g., Neal & Abreu, 2009).

4.3.2 Interpretations

By merging dip-corrected and projected surfaces from each structural region into a unified model, the heterogeneity of geological orientations across the outcrop is more accurately restored (Figure 4C). This includes distinctively flat topset and bottomset surfaces (e.g., Patruno et al., 2015; Patruno & Helland-Hansen, 2018) that were not observed with the other methodological approaches (Figure 4).

Consequently, the reconstructed clinoforms have topset gradients that are much shallower than the other projections used in this study, and more closely resemble those found in contemporary shelf-margin systems (Patruno et al., 2015). The foreset gradients are similar to the single projection method range, and at the upper limit of those observed in shelf-margin systems. The steep foreset gradients may be attributed to high sedimentation-rates (Hage et al., 2022), high overall sand content at Cerro Cazador (Bauer et al., 2020), or the propensity of mass-wasting deposits (Moscardelli & Wood, 2008). The results presented here suggest that multiple dip-corrected projection techniques yield clinoform architectures that better match global analogs in both magnitude and stacking patterns.

Table 1 summarizes measured clinoform geometries from the multiple corrections method within this study alongside comparative values from Hage et al. (2022) and the global dataset of shelf-prism clinoforms compiled by Patruno et al. (2015). The reconstructed surfaces in this study show lower topset dip values than those reported by Hage et al. (2022), with average topset dips ranging from 0.2 to 2.3°, compared to 1.7 to 3.1°. The foresets reconstructed here, ranging from 5.6 to 7.6°, also fall within the global dataset where gradients range from 0.9 to 9.8°. Notably, in clinoforms 1 through 3, foreset dips in this study steepen as the basin prograded southward, contrasting with Hage et al.'s (2022) reconstruction, which showed slight shallowing over the same interval. Bottomset geometries and dips remain consistent across datasets, with all studies showing dips under 1.5°.

5 Discussion

Restoring original depositional geometries using dip-correction methods was important for our interpretations of the DOM at Cerro Cazador, enabling comparison with other outcrop and seismic-reflection datasets (e.g., Figure 5A). The accurate representation of clinoform scale and geometry is crucial as they are direct indicators of paleoenvironmental conditions and their trajectories show how the shelf-margin evolved over geological time (Helland-Hansen & Hampson, 2009; Steel & Olsen, 2002). Through careful reconstruction of depositional geometries at Cerro Cazador, we better understand the environmental settings that influenced ancient shelf-margin systems, providing insights into paleo-water depth, sediment supply and distribution, basin dynamics, base-level changes, and sedimentary processes at the time of deposition. For example, the measurement between flat topset strata and flat bottomset strata provides a minimum measurement of paleo-basin-margin relief, or water depth, which was several hundred meters

Table 1 – Quantitative comparisons between single projection (Hage et al., 2022), multiple combined projections (this study), and collated shelf-edge clinoform data from Patruno et al. (2015).

Hage et al. (2022)		**Length** (m)	**Height** (m)	**Average Dip** (°)
Clinoform 1	Topset	840.73	44.24	3.0
	Foreset	1 566.50	283.79	10.3
	Bottomset	2 105.11	27.54	0.7
Clinoform 2	Topset	1 021.36	55.92	3.1
	Foreset	1 950.78	358.08	10.4
	Bottomset	2 246.32	27.54	0.7
Clinoform 3	Topset	2 849.44	85.14	1.7
	Foreset	2 134.68	351.41	9.3
	Bottomset	2 055.84	43.41	1.2
Clinoform 4	Topset	3 868.67	163.60	2.4
	Foreset	2 525.49	297.99	6.7
	Bottomset	1 691.30	43.41	1.5
Patruno et al. (2015)				
Shelf Edge Clinoforms	Topset	120 to 10 000	6 to 110	0.01 to 3
	Foreset	1 700 to 13 000	95 to 300	0.35 to 6.5
	Bottomset	350 to 8 500	13 to 58	0.12 to 2.8
This Study				
Clinoform 1	Topset	1 073.90	42.57	2.3
	Foreset	1 642.08	160.26	5.6
	Bottomset	2 748.82	28.38	0.6
Clinoform 2	Topset	1 251.43	21.70	1.0
	Foreset	2 075.57	232.88	6.4
	Bottomset	2 738.93	43.41	0.9
Clinoform 3	Topset	21 586.23	5.85	0.2
	Foreset	2 200.37	291.87	7.6
	Bottomset	2 883.46	42.01	0.8
Clinoform 4	Topset	2 380.96	61.77	1.5
	Foreset	2 466.38	253.75	5.9
	Bottomset	1 047.63	21.70	1.2

based on the projected cross section (Patruno et al., 2015). It is also important to distinguish which components of structural overprint are addressed by this method. The region-based correction and projection workflow corrects (i) spatially variable rigid-body rotation/tilting of bedding attitudes that otherwise causes apparent surface convergence/crossovers and biased topset/foreset dips in long transects (Figure 5B), and (ii) projection-related distortions that arise when surfaces are viewed obliquely relative to depositional dip. However, the method does not restore strain-related changes to bed geometry, including layer-parallel shortening or extension, fold-related bed thickening or thinning, or other penetrative deformation effects that modify bed length, thickness, continuity, or volume.

The different methods tested result in reconstructions that differ considerably in their geometry and thus their paleoenvironmental implications (Figure 5). Strike and dip measurements typically varied up to c. 5 to 10° every 2 to 4 km southward along the study transect. In this study, we adopted established shelf-prism clinoform models in which topsets are expected to be flat to gently dipping (typically < 2°) and foresets define the steeper depositional slope (commonly < 6°), consistent with global modern and ancient compilations (Patruno et al., 2015). We use these ranges as first-order bounds when evaluating reconstructed depositional geometries from the DOM. However, localized variations in dips may reflect genuine depositional gradient, incomplete structural correction, or local post-depositional deformation and are therefore interpreted conservatively rather than assumed to be purely artifactual.

We found that when such variations were considered (i.e., multi-correction method), clinoform slopes were accurately represented and comparable to established examples (e.g., Patruno & Helland-Hansen, 2018), validating that they were accurately represented. For example, clinoform trajectory derived from a single correction (Figure 5C) revealed an aggradational-to-progradational clinoform trajectory trend followed by a degradational phase, implying a rise and fall in base-level (Neal & Abreu, 2009). However, the multi-correction method (Figure 5D) only shows the aggradation-to-progradational phase with no degradation, implying a sea-level rise followed by relative base-level stasis. The clinoform morphology presented by the different projection models also varied substantially. Where no correction was applied, it was difficult to differentiate clinoforms. With a single correction, the topsets of clinoforms were anomalously steep (1.7 to 3.1°), which would imply unique depositional conditions unlike other ancient and modern-day depositional systems (e.g., Patruno et al., 2015). Using the multiple projection method, clinoform geometries were comparable to other foreland basin examples including the Brookian clinoforms of the North Slope, Alaska (Houseknecht & Schenk, 2005), the Lewis Shale in the Western Interior Seaway (Carvajal & Steel, 2006; Pyles & Slatt, 2000), and the Sobrarbe delta complex in the Ainsa Basin, Spain (Dreyer et al., 1999). These systems exhibit similar large-scale clinoform geometries that reflect sustained sediment delivery into subsiding foreland settings.

5.1 Future Applications

Cerro Cazador represents a case-study to understand the depositional architecture and stratigraphy of clinoforms. Given the large-scale and continuous exposure at Cerro Cazador, drone-based mapping must be corroborated by in-person, field-based methods, such as on-foot surface tracing, precise strike and dip measurements, paleoflow observations, and detailed close-up photography, to ensure data accuracy. This methodology of drone-based mapping, and subsequent geometric corrections (Figure 5D) are not only relevant for the inclination of surfaces but also thickness of sedimentary units, trajectory analyses, bedform analyses, and structural orientations, for example. Cerro Cazador exemplifies a large outcrop with some topographic and structural complexity, and well-documented regional context. We found that the outcrop was best captured using a combination of DOM and field observations (e.g., sedimentary sections and photographs). However, for other studies each researcher will need to consider their specific research objectives and outcrop characteristics such as its size, level of documentation, accessibility, and complexity to determine the appropriate mapping technique. At Cerro Cazador, subdivision into separate structural domains became warranted where bedding orientation changed appreciably along the transect, with inter-domain differences on the order of c. 20° in strike and c. 5° in dip. Although these thresholds are outcrop-specific rather than universally transferable, they provide a practical first-order guide for identifying when a single projection may no longer adequately represent local structural variability and when an

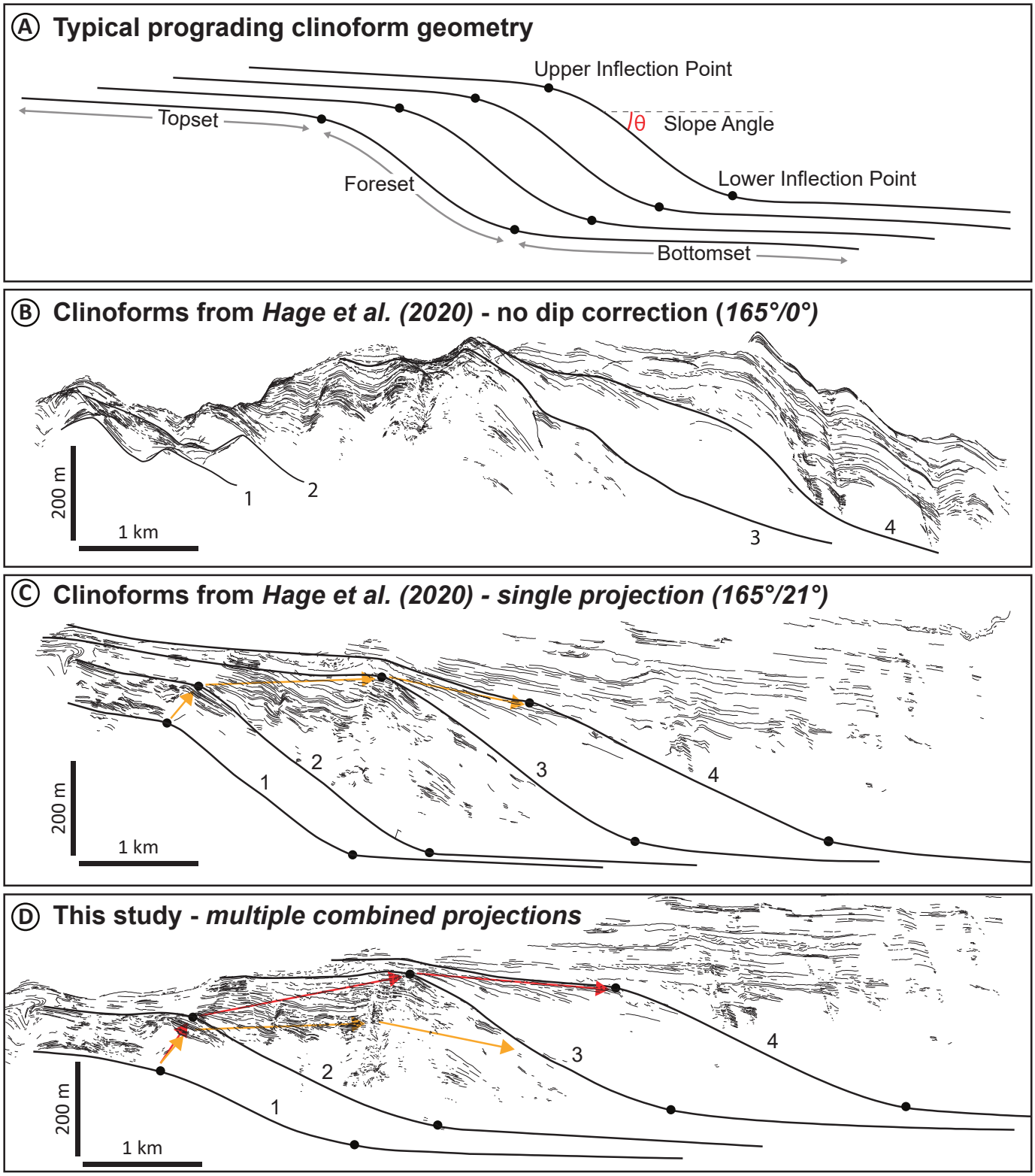

Figure 5 – Comparison of clinoform geometries using different projection methods. **(A)** Conceptual illustration of a typical prograding clinoform, with flat topset, dipping foreset, and flat bottomset separated by upper and lower inflection points. The foreset slope angle is measured between these inflection points. **(B)** No correction – strike of 165° and dip of 0°: Clinoform surfaces from Hage et al. (2022) displayed without geometric correction. The resulting geometries are unrealistic, with surfaces appearing to project uphill and no clear separation between topsets and foresets. **(C)** Single correction – strike of 165° and dip of 21°: A uniform projection applied to all clinoforms (Hage et al., 2022) improves surface clarity and reveals a clearer clinoform trajectory. Orange arrows mark the upper inflection points, showing a progradational to aggradational stacking pattern from clinoforms 1 to 3, followed by a degradational shift between 3 to 4. **(D)** Multiple corrections – Four region-specific strike and dip projections: This study's approach applies localized corrections along four structural regions. Clinoform geometries are more laterally continuous, with red arrows showing a consistent progradational-aggradational trajectory from clinoforms 1 to 3 and continued progradation into the basin from 3 to 4. Clinoforms appear longer and lower in height than those in the single correction, more closely resembling global shelf-margin analogs.

additional correction domain may be needed. For drone-based mapping, field data such as strike and dip measurements is critical (if available) to understand the structural complexity of the area, which in turn informs the choice of correction method. Field-based measurements, including precise strike and dip readings and paleoflow orientations, provide essential ground truth data that calibrates and validates interpretations derived from DOMs, allowing for more accurate representations of true surface geometries. For large-scale outcrops (> 3 km) exhibiting significant strike and dip variations, it is crucial to undertake comprehensive field measurements across the entire outcrop. These measurements are akin to ground control points (GCPs; $n = 30$) and are essential for calibrating the dip-correction process, ensuring that DOMs reflect true depositional orientations. At Cerro Cazador, these dip corrections were made at approximately 2 to 4 km intervals along the outcrop transect, though this would vary with the tectonism and extent of the region.

In extensively studied strata where depositional environments are well-constrained it will be easier to assess the accuracy of projections. Multiple corrections may be possible and can improve the accuracy of interpretations, especially in structurally complex areas. However, such comprehensive methods might not be necessary or suitable in sparsely documented or smaller study areas. This balance between methodological rigor and practical application encourages researchers to adapt standard methods to their specific conditions and objectives, ensuring both the feasibility of the study and the accuracy of the geological interpretations.

Geoscientists are predisposed to interpretation of stratigraphy in strike-oriented sections (i.e., perpendicular to paleoflow), or dip-oriented sections (i.e., parallel to paleoflow). Data projection methods, as applied in this study are most useful when projections are near parallel (± 25°) to dip or strike (e.g., Figure 2C). In this study, the application of the projection method benefitted from the approximate dip-oriented exposure of the outcrop belt (e.g., Englert et al., 2024; Nesbit et al., 2021). Other studies have shown the benefit of projections in near-strike-oriented outcrop exposures (e.g., Coutts et al., 2024).

In cases where the exposure is highly oblique to depositional dip or strike, projected stratal geometries could lead to erroneous interpretations of stratigraphic surfaces (i.e., lengthening and shortening) and stacking patterns. For example, along strike some geometries change very quickly, like channel bodies, and so by projecting on a dip profile stratigraphic architectures and geometries will be obscured. While projection methods have proven effective in ideally-oriented outcrops, application in oblique sections should be approached with caution. In outcrops with three-dimensionality, pre-projection bed length or bed-surface area may differ because points are projected along a user-defined dip-direction vector onto a 2-D plane (i.e., a shear/oblique projection), apparent lengths in the composite section may be systematically shortened or elongated depending on the angle between the outcrop/feature orientation and the projection direction. However, the corrected section should better represent stratigraphic geometry in the selected projection direction.

6 Conclusions

This study demonstrates a field-calibrated workflow that integrates UAV-derived Digital Outcrop Models (DOMs) with structural measurements to correct for outcrop perspective and deformation. The projection method allows us to produce geometrically accurate stratigraphic cross-sections to get quantifiable and reliable surface lengths, heights, and dips. A 15 km-long Upper Cretaceous exposure of shelf and shelf-margin strata in southern Chile is used to test and compare three projection approaches. The multi-correction workflow, which applies localized dip corrections across four structural regions of the outcrop, most accurately restores depositional geometry in the projected stratigraphic cross-section. Reconstructed clinoforms show gently dipping topsets (0.2 to 2.3°), foresets typical of shelf-margin slopes (5.6 to 7.6°), and flat bottomsets (< 1.5°), closely matching global datasets.

The methodological approach eliminates distortions such as stratigraphic surface convergence and uniform steepening introduced by single-correction methods in the projected cross-section. The resulting cross-section restores continuous sigmoidal clinoforms, improves the definition of shelf-edge trajectories, and yields realistic length and height relationships comparable to globally-compiled analogs. These outcomes strengthen quantitative interpretations of

shelf-margin evolution and sedimentary architecture in the Cerro Cazador study area.

Future applications should incorporate region-specific dip corrections in structurally variable outcrops exceeding several kilometers, supported by dense, spatially distributed field control. When integrated with measured sections and paleoflow data, this workflow provides a robust, reproducible framework for reconstructing depositional geometries in complex sedimentary successions.

Acknowledgements

We are grateful for D. Francisco, L. Cárdenas and A. Cárdenas at Rincon Negro Ranch as well as Jose, Luis, and Manuel at San Luis Ranch for allowing us to access their lands. We also thank the Alvarez–Roehrs family for our stay at Hotel Tres Pasos.

Data and code availability

Our data and code can be found at the following free repository: `https://github.com/ThomasPeploe/DOM-Corrections`.

Conflict of interest statement

The authors declare no conflict of interest.

Production manager note: As of publication date, RGE is a current member of the Sedimentologika Steering Committee. RGE has not been involved with any of the editorial process of this paper.

Artificial intelligence use statement

All research, analysis, writing, and editing were performed without generative AI assistance.

Funding

Support for this research was provided by a Natural Sciences and Engineering Research Council of Canada Discovery Grant (RGPIN-2018-04223) held by S.M.H., doctoral sponsorship of T.G.E.P. by ConocoPhillips Alaska, alongside the sponsors of the Chile Slope Systems Joint Industry Project (Woodside, Apache, Petrobras, CNOOC-Nexen, BP, and ConocoPhillips).

Citing this Research Article

To cite this paper use the following information:

Authors

Thomas G. E. Peploe, Paul R. Nesbit, Rebecca G. Englert, Miquel Poyatos-Moré, Brian W. Romans, Lisa Stright, Stephen M. Hubbard

Title

Integrating field-based and digital datasets to improve geometric accuracy of geologic cross sections constructed from outcrop

Short Title

Improving geometric accuracy of geologic cross sections

Publishing Information

Publication: Sedimentologika
Volume: 4
Issue: 2
Year: 2026
DOI: 10.57035/journals/sdk.2026.e42.2385
Language: en
License: CC-BY 4.0

References

Bauer, D. B., Hubbard, S. M., Covault, J. A., & Romans, B. W. (2020). Inherited Depositional Topography Control on Shelf-Margin Oversteepening, Readjustment, and Coarse-Grained Sediment Delivery to Deep Water, Magallanes Basin, Chile. *Frontiers in Earth Science*, *7*, 1–22. https://doi.org/10.3389/feart.2019.00358

Bellian, J. A., Kerans, C., & Jennette, D. C. (2005). Digital Outcrop Models: Applications of Terrestrial Scanning Lidar Technology in Stratigraphic Modeling. *Journal of Sedimentary Research*, *75*(2), 166–176. https://doi.org/10.2110/jsr.2005.013

Bemis, S. P., Micklethwaite, S., Turner, D., James, M. R., Akciz, S., Thiele, S. T., & Bangash, H. A. (2014). Ground-based and UAV-Based photogrammetry: A multi-scale, high-resolution mapping tool for structural geology and paleoseismology. *Journal of Structural Geology*, *69*, 163–178. https://doi.org/10.1016/j.jsg.2014.10.007

Bistacchi, A., Balsamo, F., Storti, F., Mozafari, M., Swennen, R., Solum, J., Tueckmantel, C., & Taberner, C. (2015). Photogrammetric digital outcrop reconstruction, visualization with textured surfaces, and three-dimensional structural analysis and modeling: Innovative methodologies applied to fault-related dolomitization (Vajont Limestone, Southern Alps, Italy). *Geosphere*, *11*(6), 2031–2048. https://doi.org/10.1130/GES01005.1

Campana, S. (2017). Drones in Archaeology. State-of-the-art and Future Perspectives. *Archaeological Prospection*, *24*(4), 275–296. https://doi.org/10.1002/arp.1569

Carvajal, C. R., & Steel, R. J. (2006). Thick turbidite successions from supply-dominated shelves during sea-level highstand. *Geology*, *34*(8), 665–668. https://doi.org/10.1130/G22505.1

Casini, G., Hunt, D. W., Monsen, E., & Bounaim, A. (2016). Fracture characterization and modeling from virtual outcrops. *AAPG Bulletin*, *100*(1), 41–61. https://doi.org/10.1306/09141514228

Cawood, A. J., Bond, C. E., Howell, J. A., Butler, R. W. H., & Totake, Y. (2017). LiDAR, UAV or compass-clinometer? Accuracy, coverage and the effects on structural models. *Journal of Structural Geology*, *98*, 67–82. https://doi.org/10.1016/j.jsg.2017.04.004

Chesley, J. T., Leier, A. L., White, S., & Torres, R. (2017). Using unmanned aerial vehicles and structure-from-motion photogrammetry to characterize sedimentary outcrops: An example from the Morrison Formation, Utah, USA. *Sedimentary Geology*, *354*, 1–8. https://doi.org/10.1016/j.sedgeo.2017.03.013

Coutts, D., Hubbard, S., Englert, R., Ward, P., & Matthews, W. (2024). Dissecting 20 million years of deep-water forearc sediment routing using an integrated basin-wide Bayesian chronostratigraphic framework. *GSA Bulletin*, *136*(9–10), 3485–3509. https://doi.org/10.1130/B37194.1

Daniels, B. G., Auchter, N. C., Hubbard, S. M., Romans, B. W., Matthews, W. A., & Stright, L. (2018). Timing of deep-water slope evolution constrained by large-n detrital and volcanic ash zircon geochronology, Cretaceous Magallanes Basin, Chile. *GSA Bulletin*, *130*(3–4), 438–454. https://doi.org/10.1130/B31757.1

Daniels, B. G., Hubbard, S. M., Romans, B. W., Malkowski, M. A., Matthews, W. A., Bernhardt, A., Kaempfe, S. A., Jobe, Z. R., Fosdick, J. C., Schwartz, T. M., Fildani, A., & Graham, S. A. (2019). Revised chronostratigraphic framework for the Cretaceous Magallanes-Austral Basin, Última Esperanza Province, Chile. *Journal of South American Earth Sciences*, *94*, 102209. https://doi.org/10.1016/j.jsames.2019.05.025

Dreyer, T., Corregidor, J., Arbues, P., & Puigdefabregas, C. (1999). Architecture of the tectonically influenced Sobrarbe deltaic complex in the Ainsa Basin, northern Spain. *Sedimentary Geology*, *127*(3–4), 127–169. https://doi.org/10.1016/S0037-0738(99)00056-1

Durkin, P. R., Hubbard, S. M., Holbrook, J., Weleschuk, Z., Nesbit, P., Hugenholtz, C., Lyons, T., & Smith, D. G. (2020). Recognizing the product of concave-bank sedimentary processes in fluvial meander-belt strata. *Sedimentology*, *67*(6), 2819–2849. https://doi.org/10.1111/sed.12743

Enge, H. D., Buckley, S. J., Rotevatn, A., & Howell, J. A. (2007). From outcrop to reservoir simulation model: Workflow and procedures. *Geosphere*, *3*(6), 469–490. https://doi.org/10.1130/GES00099.1

Englert, R. G., Hubbard, S. M., Coutts, D. S., & Matthews, W. A. (2018). Tectonically controlled initiation of contemporaneous deep-water channel systems along a Late Cretaceous continental margin, western British Columbia, Canada. *Sedimentology*, *65*(7), 2404–2438. https://doi.org/10.1111/sed.12472

Englert, R. G., Hubbard, S. M., Romans, B. W., Kaempfe, S., Bell, D., Nesbit, P. R., & Stright, L. (2024). Flow dynamics as Froude-supercritical turbidity currents encounter metre-scale slope minibasin topography. *Depositional Record*, *10*(5), 527–558. https://doi.org/10.1002/dep2.262

Fildani, A., & Hessler, A. M. (2005). Stratigraphic record across a retroarc basin inversion: Rocas Verdes–Magallanes Basin, Patagonian Andes, Chile. *Geological Society of America Bulletin*, *117*(11), 1596. https://doi.org/10.1130/B25708.1

Fosdick, J. C., Romans, B. W., Fildani, A., Bernhardt, A., Calderón, M., & Graham, S. A. (2011). Kinematic evolution of the Patagonian retroarc fold-and-thrust belt and Magallanes foreland basin, Chile and Argentina, 51°30′S. *GSA Bulletin*, *123*(9–10), 1679–1698. https://doi.org/10.1130/B30242.1

Gilbert, G. K. (1885). *The Topographic Features of Lake Shores*. U.S. Government Printing Office.

Hage, S., Romans, B. W., Peploe, T. G. E., Poyatos-Moré, M., Haeri Ardakani, O., Bell, D., Englert, R. G., Kaempfe-Droguett, S. A., Nesbit, P. R., Sherstan, G., Synnott, D. P., & Hubbard, S. M. (2022). High rates of organic carbon burial in submarine deltas maintained on geological timescales. *Nature Geoscience*, *15*(11), 919–924. https://doi.org/10.1038/s41561-022-01048-4

Helland-Hansen, W., & Hampson, G. J. (2009). Trajectory analysis: concepts and applications. *Basin Research*, *21*(5), 454–483. https://doi.org/10.1111/j.1365-2117.2009.00425.x

Hodgetts, D. (2013). Laser scanning and digital outcrop geology in the petroleum industry: A review. *Marine and Petroleum Geology*, *46*, 335–354. https://doi.org/10.1016/j.marpetgeo.2013.02.014

Honarmand, M., & Shahriari, H. (2021). Geological Mapping Using Drone-Based Photogrammetry: An Application for Exploration of Vein-Type Cu Mineralization. *Minerals*, *11*(6), 585. https://doi.org/10.3390/min11060585

Houseknecht, D. W., & Schenk, C. J. (2005). Sedimentology and sequence stratigraphy of the Cretaceous Nanushuk, Seabee, and Tuluvak formations exposed on Umiat Mountain, north-central Alaska. *Professional Paper*, Article 1709-B. https://doi.org/10.3133/pp1709B

Hubbard, S. M., Fildani, A., Romans, B. W., Covault, J. A., & McHargue, T. R. (2010). High-Relief Slope Clinoform Development: Insights from Outcrop, Magallanes Basin, Chile. *Journal of Sedimentary Research*, *80*(5), 357–375. https://doi.org/10.2110/jsr.2010.042

Jones, R. R., McCaffrey, K. J. W., Clegg, P., Wilson, R. W., Holliman, N. S., Holdsworth, R. E., Imber, J., & Waggott, S. (2009). Integration of regional to outcrop digital data: 3D visualisation of multi-scale geological models. *Computers & Geosciences, 3D Modeling in Geology*, *35*(1), 4–18. https://doi.org/10.1016/j.cageo.2007.09.007

Katz, H. R. (1963). Revision of Cretaceous Stratigraphy in Patagonian Cordillera of Ultima Esperanza, Magallanes Province, Chile. *AAPG Bulletin*, *47*(3), 506–524. https://doi.org/10.1306/BC743A5D-16BE-11D7-8645000102C1865D

Kirsch, M., Lorenz, S., Zimmermann, R., Tusa, L., Möckel, R., Hödl, P., Booysen, R., Khodadadzadeh, M., & Gloaguen, R. (2018). Integration of Terrestrial and Drone-Borne Hyperspectral and Photogrammetric Sensing Methods for Exploration Mapping and Mining Monitoring. *Remote Sensing*, *10*(9), 31. https://doi.org/10.3390/rs10091366

Kucharczyk, M., & Hugenholtz, C. H. (2021). Remote sensing of natural hazard-related disasters with small drones: Global trends, biases, and research opportunities. *Remote Sensing of Environment*, *264*, 112577. https://doi.org/10.1016/j.rse.2021.112577

Magnani, M., Douglass, M., Schroder, W., Reeves, J., & Braun, D. R. (2020). The Digital Revolution to Come: Photogrammetry in Archaeological Practice. *American Antiquity*, *85*(4), 737–760. https://doi.org/10.1017/aaq.2020.59

McCaffrey, K. J. W., Hodgetts, D., Howell, J., Hunt, D., Imber, J., Jones, R. R., Tomasso, M., Thurmond, J., & Viseur, S. (2010). Virtual fieldtrips for petroleum geoscientists. *Geological Society, London, Petroleum Geology Conference Series*, *7*(1), 19–26. https://doi.org/10.1144/0070019

Moscardelli, L., & Wood, L. (2008). New classification system for mass transport complexes in offshore Trinidad. *Basin Research*, *20*(1), 73–98. https://doi.org/10.1111/j.1365-2117.2007.00340.x

Mutti, E., & Ricci-Lucchi, F. (1978). Turbidites of the northern Apennines: introduction to facies analysis. *International Geology Review*, *20*(2), 125–166. https://doi.org/10.1080/00206817809471524

Neal, J., & Abreu, V. (2009). Sequence stratigraphy hierarchy and the accommodation succession method. *Geology*, *37*(9), 779–782. https://doi.org/10.1130/G25722A.1

Nesbit, P. R., Durkin, P. R., Hugenholtz, C. H., Hubbard, S. M., & Kucharczyk, M. (2018). 3-D stratigraphic mapping using a digital outcrop model derived from UAV images and structure-from-motion photogrammetry. *Geosphere*, *14*(6), 2469–2486. https://doi.org/10.1130/GES01688.1

Nesbit, P. R., Hubbard, S. M., Daniels, B. G., Bell, D., Englert, R. G., & Hugenholtz, C. H. (2021). Digital re-evaluation of down-dip channel-fill architecture in deep-water slope deposits: Multi-scale perspectives from UAV-SfM. *Depositional Record*, *7*(3), 480–499. https://doi.org/10.1002/dep2.137

Nesbit, P. R., & Hugenholtz, C. H. (2019). Enhancing UAV–SfM 3D Model Accuracy in High-Relief Landscapes by Incorporating Oblique Images. *Remote Sensing*, *11*(3), 24. https://doi.org/10.3390/rs11030239

Nieminski, N. M., & Graham, S. A. (2017). Modeling Stratigraphic Architecture Using Small Unmanned Aerial Vehicles and Photogrammetry: Examples From the Miocene East Coast Basin, New Zealand. *Journal of Sedimentary Research*, *87*(2), 126–132. https://doi.org/10.2110/jsr.2017.5

Niethammer, U., James, M. R., Rothmund, S., Travelletti, J., & Joswig, M. (2012). UAV-based remote sensing of the Super-Sauze landslide: Evaluation and results. *Engineering Geology, Integration of Technologies for Landslide Monitoring and Quantitative Hazard Assessment*, *128*, 2–11. https://doi.org/10.1016/j.enggeo.2011.03.012

Park, S., & Choi, Y. (2020). Applications of Unmanned Aerial Vehicles in Mining from Exploration to Reclamation: A Review. *Minerals*, *10*(8), 663. https://doi.org/10.3390/min10080663

Patruno, S., Hampson, G. J., & Jackson, C. A.-L. (2015). Quantitative characterisation of deltaic and subaqueous clinoforms. *Earth-Science Reviews*, *142*, 79–119. https://doi.org/10.1016/j.earscirev.2015.01.004

Patruno, S., & Helland-Hansen, W. (2018). Clinoforms and clinoform systems: Review and dynamic classification scheme for shorelines, subaqueous deltas, shelf edges and continental margins. *Earth-Science Reviews*, *185*, 202–233. https://doi.org/10.1016/j.earscirev.2018.05.016

Pellegrini, C., Patruno, S., Helland-Hansen, W., Steel, R. J., & Trincardi, F. (2020). Clinoforms and clinothems: Fundamental elements of basin infill. *Basin Research*, *32*(2), 187–205. https://doi.org/10.1111/bre.12446

Posamentier, H. W., & Walker, R. G. (Eds.). (2006). *Facies Models Revisited: SEPM Special Publication: 84*. SEPM Society for Sedimentary Geology. https://doi.org/10.2110/pec.06.84

Pringle, J. K., Howell, J. A., Hodgetts, D., Westerman, A. R., & Hodgson, D. M. (2006). Virtual outcrop models of petroleum reservoir analogues: a review of the current state-of-the-art. *First Break*, *24*(3). https://doi.org/10.3997/1365-2397.2006005

Pyles, D. R., & Slatt, R. M. (2000). A High Frequency Sequence Stratigraphic Framework for Shallowthrough Deep-Water Deposits of the Lewis Shale and Fox Hills Sandstone, Great Divide and Washakie Basins, Wyoming. In P. Weimer (Ed.), *Deep-Water Reservoirs of the World* (Vol. 20, p. 0). SEPM Society for Sedimentary Geology. https://doi.org/10.5724/gcs.00.15.0836

Renard, F., Voisin, C., Marsan, D., & Schmittbuhl, J. (2006). High resolution 3D laser scanner measurements of a strike-slip fault quantify its morphological anisotropy at all scales. *Geophysical Research Letters*, *33*(4). https://doi.org/10.1029/2005GL025038

Rich, J. L. (1951). Three critical environments of deposition, and criteria for recognition of rocks deposited in each of them. *GSA Bulletin*, *62*(1), 1–20. https://doi.org/10.1130/0016-7606(1951)62[1:TCEODA]2.0.CO;2

Romans, B. W., Fildani, A., Graham, S. A., Hubbard, S. M., & Covault, J. A. (2010). Importance of predecessor basin history on sedimentary fill of a retroarc foreland basin: provenance analysis of the Cretaceous Magallanes basin, Chile (50-52°S): Importance of predecessor basin history on sedimentary. *Basin Research*, *22*(5), 640–658. https://doi.org/10.1111/j.1365-2117.2009.00443.x

Sachse, V. F., Strozyk, F., Anka, Z., Rodriguez, J. F., & Di Primio, R. (2016). The tectono-stratigraphic evolution of the Austral Basin and adjacent areas against the background of Andean tectonics, southern Argentina, South America. *Basin Research*, *28*(4), 462–482. https://doi.org/10.1111/bre.12118

Schwartz, T. M., Fosdick, J. C., & Graham, S. A. (2017). Using detrital zircon U-Pb ages to calculate Late Cretaceous sedimentation rates in the Magallanes-Austral basin, Patagonia. *Basin Research*, *29*(6), 725–746. https://doi.org/10.1111/bre.12198

Shahmoradi, J., Talebi, E., Roghanchi, P., & Hassanalian, M. (2020). A Comprehensive Review of Applications of Drone Technology in the Mining Industry. *Drones*, *4*(3), 34. https://doi.org/10.3390/drones4030034

Sikakwe, G. U. (2023). Mineral exploration employing drones, contemporary geological satellite remote sensing and geographical information system (GIS) procedures: A review. *Remote Sensing Applications: Society and Environment*, *31*, 100988. https://doi.org/10.1016/j.rsase.2023.100988

Steel, R. J., Crabaugh, J., Schellpeper, M., Mellere, D., Plink-Bjorklund, P., Deibert, J., & Loeseth, T. (2000). Deltas vs. Rivers on the Shelf Edge: Their Relative Contributions to the Growth of Shelf-Margins and Basin-Floor Fans (Barremian and Eocene, Spitsbergen). In P. Weimer (Ed.), *Deep-Water Reservoirs of the World* (Vol. 20). SEPM (Society for Sedimentary Geology). https://doi.org/10.5724/gcs.00.15.0981

Steel, R. J., & Olsen, T. (2002). Clinoforms, Clinoform Trajectories and Deepwater Sands. In J. Armentrout (Ed.), *Sequence Stratigraphic Models for Exploration and Production: Evolving Methodology, Emerging Models, and Application Histories: 22nd Annual* (pp. 367–380). SEPM. https://doi.org/10.5724/gcs.02.22

Thompson, E. M., & Worden, C. B. (2017). Estimating Rupture Distances without a Rupture. *Bulletin of the Seismological Society of America*, *108*(1), 371–379. https://doi.org/10.1785/0120170174

Wakeford, Z. E., Chmielewska, M., Hole, M. J., Howell, J. A., & Jerram, D. A. (2019). Combining thermal imaging with photogrammetry of an active volcano using UAV: an example from Stromboli, Italy. *Photogrammetric Record*, *34*(168), 445–466. https://doi.org/10.1111/phor.12301

Wilson, T. J. (1991). Transition from back-arc to foreland basin development in the southernmost Andes: Stratigraphic record from the Ultima Esperanza District, Chile. *GSA Bulletin*, *103*(1), 98–111. https://doi.org/10.1130/0016-7606(1991)103<0098:TFBATF>2.3.CO;2

Zambrano, J. J., & Urien, C. M. (1970). Geological outline of the basins in southern Argentina and their continuation off the Atlantic shore. *Journal of Geophysical Research*, *75*(8), 1363–1396. https://doi.org/10.1029/JB075i008p01363